Three-dimensional quantitative T1 and T2 mapping of the carotid artery: Sequence design and in vivo feasibility

Coolen, BF; Poot, DHJ; Liem, MI; Smits, LP; Gao, S; Kotek, G; Klein, S; Nederveen, AJ

DOI
10.1002/mrm.25634

Publication date
2016

Document Version
Final published version

Published in
Magnetic Resonance in Medicine

Magnetic Resonance in Medicine 75:1008–1017 (2016)

Three-Dimensional Quantitative T_1 and T_2 Mapping of the Carotid Artery: Sequence Design and In Vivo Feasibility

Bram F. Coolen,[1†*] Dirk H.J. Poot,[2,3†] Madieke I. Liem,[4] Loek P. Smits,[5] Shan Gao,[6] Gyula Kotek,[7] Stefan Klein,[2] and Aart J. Nederveen[1]

Purpose: A novel three-dimensional (3D) T_1 and T_2 mapping protocol for the carotid artery is presented.

Methods: A 3D black-blood imaging sequence was adapted allowing carotid T_1 and T_2 mapping using multiple flip angles and echo time (TE) preparation times. B_1 mapping was performed to correct for spatially varying deviations from the nominal flip angle. The protocol was optimized using simulations and phantom experiments. In vivo scans were performed on six healthy volunteers in two sessions, and in a patient with advanced atherosclerosis. Compensation for patient motion was achieved by 3D registration of the inter/intrasession scans. Subsequently, T_1 and T_2 maps were obtained by maximum likelihood estimation.

Results: Simulations and phantom experiments showed that the bias in T_1 and T_2 estimation was $< 10\%$ within the range of physiological values. In vivo T_1 and T_2 values for carotid vessel wall were 844 ± 96 and 39 ± 5 ms, with good repeatability across scans. Patient data revealed altered T_1 and T_2 values in regions of atherosclerotic plaque.

Conclusion: The 3D T_1 and T_2 mapping of the carotid artery is feasible using variable flip angle and variable TE preparation acquisitions. We foresee application of this technique for plaque characterization and monitoring plaque progression in atherosclerotic patients. **Magn Reson Med 75:1008–1017, 2016. © 2015 Wiley Periodicals, Inc.**

Key words: carotid artery; vessel wall imaging; quantitative imaging; T_1 mapping; T_2 mapping; atherosclerosis

INTRODUCTION

Recent studies on MR imaging of carotid atherosclerosis have shown strong correlations between plaque composition and subsequent cerebrovascular events (1–3). Plaque composition may even be a risk factor independent from the degree of luminal stenosis (4). Characterization of plaque components, including lipid core, calcifications, fibrous tissue and hemorrhage is currently performed using multicontrast MR imaging, in which each component has a unique combination of hyper or hypointense signal on T_1-weighted, T_2-weighted and proton density-weighted images (5–7). However, due to its qualitative nature, the reproducibility of this method will be strongly affected by several factors, such as coil positioning, sequence parameters and intra/interobserver variability (8). Alternatively, quantitative MR imaging is capable of directly measuring structural tissue parameters (T_1, T_2) and has been shown to have high reproducibility in various applications (9,10). T_1 and/or T_2 measurements are therefore considered to be valuable in longitudinal studies or when comparing results between different research sites. Additionally, this would provide the possibility to define threshold values for automatic segmentation purposes without the use of signal normalization based on reference tissues.

In current literature, quantitative relaxation measurements specifically for carotid vessel wall imaging are limited to 2D T_2 and T_2^* measurements using either multi-echo spin echo (11,12) or gradient echo (13,14) sequences, respectively. Biasiolli et al. showed that carotid T_2 mapping is able to distinguish different plaque types and could serve as an alternative method for multicontrast imaging (12). A major challenge for 3D carotid T_1 measurements is its combination with blood suppression and possible methods have only recently been presented (15,16). Commonly available T_1 mapping sequences, such as IR Look-Locker or DESPOT1 (17,18), cannot be easily used in combination with black-blood techniques. However, blood suppression is of paramount importance for visualization and analysis of the thin vessel wall.

In this study, we present a novel carotid imaging method for combined black-blood T_1 and T_2 mapping of the vessel wall with full 3D coverage and a high isotropic resolution.

In short, the method uses a three-dimensional (3D) gradient echo sequence with time efficient motion-sensitized preparation for blood suppression (19), together with variable flip angle (18) and variable TE preparation times (20,21) for combined T_1 and T_2 estimation. A major advantage is that only a small set of

[1]Department of Radiology, Academic Medical Center, Amsterdam, the Netherlands.

[2]Biomedical Imaging Group Rotterdam, Depts. of Radiology and Medical Informatics, Erasmus Medical Center, Rotterdam, the Netherlands.

[3]Quantitative Imaging Group, Department of Imaging Physics, Delft University of Technology, Delft, The Netherlands.

[4]Department of Neurology, Academic Medical Center, Amsterdam, the Netherlands.

[5]Department of Vascular Medicine, Academic Medical Center, Amsterdam, the Netherlands.

[6]Department of Radiology, Division of Image Processing, Leiden University Medical Center, Leiden, The Netherlands.

[7]Department of Radiology, Erasmus Medical Center, Rotterdam, the Netherlands.

Grant sponsor: Dutch Technology Foundation STW; Grant number: CARISMA 11631.

*Correspondence to: Bram F. Coolen, Ph.D., Department of Radiology, Academic Medical Center, PO BOX 22660, 1100 DD, Amsterdam, the Netherlands.
E-mail: b.f.coolen@amc.uva.nl

†Drs. Coolen and Poot contributed equally to this work.

Received 4 August 2014; revised 17 December 2014; accepted 5 January 2015

DOI 10.1002/mrm.25634
Published online 28 April 2015 in Wiley Online Library (wileyonlinelibrary.com).

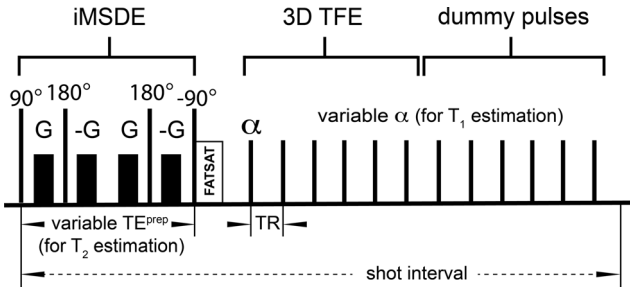

FIG. 1. Carotid artery 3D black-blood T_1 and T_2 mapping sequence. Pulse sequence diagram for carotid artery 3D black-blood T_1 and T_2 mapping. Blood suppression, as well as T_2-weighting, is achieved by an iMSDE prepulse. Subsequently, acquisition is performed using a segmented TFE read-out. T_1 can be estimated from scans with different flip angle α, while T_2 is estimated from scans with different TE^{prep} (see also Table 1). To ensure correct T_1 and T_2 quantification, after each TFE shot, steady-state conditions are restored by a series of dummy pulses. For clarity, additional gradients within the prepulse for eddy current compensation (19) are not shown. Specific parameter values are mentioned in the 'Method' section.

parameters is changed for different acquisitions, while keeping the basic sequence unchanged. The accuracy of T_1 and T_2 estimation was first evaluated with phantom experiments and simulations. Feasibility of the approach in vivo was then demonstrated in healthy volunteers, as well as in a patient with known history of carotid atherosclerosis.

METHODS

MRI Sequence Design

Figure 1 shows the basic sequence for carotid artery T_1 and T_2 mapping, which is based on a fat-suppressed radiofrequency (RF)-spoiled 3D segmented turbo field echo (TFE) acquisition with motion-sensitized preparation (iMSDE) for blood suppression. The prepulse consists of an initial 90°_x pulse, followed by two composite 180°_y pulses and finally a 90°_{-x} flipback pulse. Motion sensitized gradients with eddy current compensation are added to cause intravoxel dephasing of flowing blood, while preserving phase coherence of static tissue (19). For the static tissue, the prepulse effectively causes T_2 weighting of available longitudinal magnetization, which therefore allows for T_2 quantification when performing measurements with variable TE preparation times (TE^{prep}) (21). A key feature of the sequence is that after each TFE shot (consisting of N_α^{TFE} excitation pulses), several dummy pulses (N_α^{DUMMY}) are played out, for which no signal acquisition takes place. This ensures that T_1-weighted steady-state conditions, which are perturbed by each iMSDE prepulse, are restored after signal acquisition. T_1 quantification is then possible by performing measurements at different flip angles α (18). Table 1 shows multiple scans (no. 1–4) of the proposed method with different sequence parameters needed for T_1 and T_2 quantification. Optimal flip angles were calculated based on Deoni et al (18), assuming T_1 of sternocleidomastoid muscle (1100 ms, ref [16]) and using $f = S_{\alpha 1}/S_{max} = S_{\alpha 2}/S_{max} = 0.8$. Given our iMSDE prepulse design, a TE of 11.5 was the shortest achievable value. Other sequence parameters were identical for all scans: repetition time/echo time (TR/TE) = 10/3.7 ms, $N_\alpha^{TFE} = 32$, field of view (FOV) = 144 × 144 × 25 mm^3 (coronal), resolution = 0.7 × 0.7 × 0.7 mm^3, prepulse first-order moment (m1) = 234 $mTms^2/m$, venc = 4 cm/s, fat suppression = SPIR prepulse, bandwidth = 240 Hz/pixel, b-value (iMSDE preparation) < 1 s/mm^2.

A Cartesian k-space sampling is used, however, in a radial YZ manner where each TFE shot starts in the center of k_{YZ} space. Frequency encoding was set in head/feet direction. Also note that we chose a conservative value for N_α^{TFE} to minimize T_1 modulation of k-space and have optimal blood suppression. A startup time of 10 s was used to allow magnetization achieve pseudo steady-state conditions. No parallel imaging techniques were used. Total scan time for all 4 scans was 15 min.

All measurements were performed on a 3.0 Tesla (T) Philips Ingenia MR scanner (Philips Medical Systems, Best, the Netherlands). The gradient system allowed a maximum gradient strength of 45 mT/m on each axis. For carotid artery imaging, we used a dedicated 8-channel neck coil (Shanghai Chenguang Medical Technologies, Shanghai, China).

T_1 and T_2 Fitting

If sufficient dummy pulses are applied after read-out, a steady-state transverse magnetization is obtained that is identical to the normal TFE steady-state. Immediately after the iMSDE preparation the TFE steady-state of stationary spins is reduced by the T_2 decay during TE^{prep}. Thus, the pseudo steady-state signal as measured directly after the preparation is given by:

$$M^{SS} = A\frac{(1 - e^{-TR/T_1})\sin\alpha}{(1 - e^{-TR/T_1}\cos\alpha\ )}e^{-TE^{prep}/T_2}, \qquad [1]$$

in which "A" is a factor representing proton density, but also including T_2* effects and coil sensitivity. From scans 1–4, maps of the parameters A, T_1, and T_2, as well as the noise level σ were simultaneously obtained by maximum likelihood estimation using the methods proposed by Poot (22). This estimation takes the Rice distribution of the magnitude MR images into account:

$$\hat{\mathbf{A}},\ \hat{\mathbf{T}}_1,\ \hat{\mathbf{T}}_2, \hat{\boldsymbol{\sigma}} = \arg\max_{\mathbf{A},\mathbf{T}_1,\mathbf{T}_2,\boldsymbol{\sigma}} \sum_{\mathbf{x}}\sum_{i} \ln \left[p_{Rice}\left(M_i(\mathbf{x}), M_i^{SS}(A(\mathbf{x}), T_1(\mathbf{x}), T_2(\mathbf{x})), \sigma(\mathbf{x})\right)\right] + \lambda\, \Delta\ln(\boldsymbol{\sigma}), \qquad [2]$$

Table 1
Scan Protocol for 3D Carotid T_1 and T_2 Mapping (Nonfixed Parameters Only)

Scan no.	α [°]	TE^{prep} [ms]	N_α^{DUMMY} [-]	Acq. time [s]
1	4	11.5	150	370
2	15	11.5	50	170
3	15	26	50	170
4	15	45	50	170

where the subscript $i \in [1,\ldots,4]$ indicates the scan number, $\mathbf{x}$ the voxel location and $M_i(\mathbf{x})$ the measured intensity in scan i at voxel $\mathbf{x}$. In Eq. [2], the noise level map $\boldsymbol{\sigma}$ is spatially regularized with the laplacian (Δ) with a regularization weight $\lambda = 10$. With this regularization weight, $\boldsymbol{\sigma}$ is estimated with a standard deviation of less than 10% of the actual value. Accurate estimation of the noise level is relevant for the evaluation of the Cramér Rao Lower bound (CRLB) (22,23), which will be used to quantify the precision of the estimates. The nonlinear optimization problem in Eq. [2] was iteratively solved in partly overlapping blocks of $4 \times 4 \times 4$ voxels. This was used to improve computational efficiency and has no effect on the final solution, or on the spatial resolution of the quantitative T_1 and T_2 maps. The initialization of this nonlinear optimization and details about the optimization method are given in Appendix A.

B_1 Correction

The variable flip angle method for T_1 estimation relies on knowledge of the local flip angle (24), which is proportional to the B_1 field and may vary throughout the imaging volume. In case of imaging of the neck, these variations are especially strong at high field strength (7T), but already noticeable at 3T as well (25). To quantify the flip angle distribution, an additional B_1 mapping scan as proposed by Yarnykh (26) was performed. Unfortunately, this method has no black-blood properties and therefore poor vessel wall delineation. B_1 variations, however, are rather smooth across the imaging volume and when properly masking the acquired B_1 map, reliable flip angle scaling maps can be obtained. A detailed explanation of the B_1 mapping protocol and the incorporation into the carotid T_1 and T_2 analysis can be found in Appendix B.

Simulations

To investigate the influence of the number of dummy pulses N_α^{DUMMY} on the accuracy of T_1 and T_2 estimation as function of reference T_1 and T_2 relaxation times, simulations of the Bloch equations were performed. For this, the iMSDE preparation module was modeled as a T_2 preparation module (without gradients), in which T_2 relaxation takes place over the time interval TE^{prep}. TFE and dummy excitations are modeled as infinitely short pulses with effective flip angle α. Because of the use of RF-spoiling, only T_1 relaxation was assumed during TR. To reach the pseudo steady-state condition the first 10 s in the simulation were ignored, representative of the actual acquisition.

Phantom Measurements

To validate the accuracy of the 3D carotid T_1 and T_2 mapping sequence, phantom experiments were performed. Phantoms were constructed using previously described methods (27). In short, a gel based on Carrageenan (KC-200S: Chuo Kasei Co., Ltd., Osaka, Japan) was prepared at 100°C. Then, T_1 and T_2 values were manipulated by adding $GdCl_3$ and agarose (Sigma Aldrich, A6013 Type 1), respectively. The gels were poured into 50 ml Falcon tubes and cooled down to room temperature. The tubes were placed in a custom-built phantom holder, which was filled with water to improve shimming. T_1 and T_2 values were determined using the proposed protocol for carotid artery T_1 and T_2 mapping (see section "Volunteer study") with and without additional B_1 mapping. Additionally, T_1 and T_2 reference values were determined using an Inversion Recovery Look Locker sequence (TR/TE = 10/3.7 ms, ΔTI = 80 ms, $\alpha = 8°$, cycle repetition time = 10 s) and multiecho spin-echo sequence (TR = 2s, ΔTE = 6 ms), respectively.

Volunteer Study

The institutional review board of our hospital approved this study. All subjects gave written informed consent for participating in this study. To obtain reference carotid T_1 and T_2 values and to assess the repeatability of the proposed method, six healthy volunteers (30 ± 6 years) were scheduled for MRI at two different days with the following protocol. After scout scans, a time-of-flight multislice MRA was used to visualize the carotid arteries. Then, a 3D volume together with volume shim boxes were positioned in the high SNR regions covering both carotid arteries and muscle. First, a non–RF-spoiled 3D iMSDE black-blood reference scan (TFE factor = 80, number of averages = 2, acquisition time = 2 min 30 s) was acquired for registration purposes (see "In vivo data analysis"). Subsequently, T_1-weighted and T_2-weighted images (scan 1–4) were acquired according to the parameters in Table 1. To correct for spatial variations of the prescribed flip angle, B_1 mapping was performed in the same FOV using the actual flip angle method proposed by Yarnykh (26) with the following parameters: TR1/TR2 = 100/20 ms, TE = 3.7s nominal flip angle = 50°, resolution = $1.4 \times 1.4 \times 1.4$ mm, acquisition time = 5 min. We instructed our subjects to only swallow between scan, which ensured good image quality in most cases. In other cases (5–10%) when abrupt motion during the scan had occurred, the scan was repeated. The typical MRI session duration was around 45 min.

In addition to the previous experiment, a patient (81 years) with known history of carotid atherosclerosis was scanned to see whether regions of plaque were associated with changes in carotid T_1 and/or T_2 values.

In Vivo Data Analysis

Registration of Intra/Intersession Scans

Scans 1–4 were registered to the 3D iMSDE reference scan using the open source Elastix image registration software (28). We used the 3D iMSDE reference scan as a target to avoid bias to any of the scans used for the quantification. The registration was performed in 3D, using a nonrigid B-spline transformation model with a control point spacing of 15 mm, with mutual information as a similarity measure, in a region of interest (ROI) around the carotid as recommended in (29).

The registration ROI was drawn approximately 10 mm around the common carotid, close to the bifurcation. This ROI was extended in (up–down) direction. It was

manually verified that the registration successfully mapped the quantification scans to the anatomical scans within this ROI. If the registration was not successful, slight modifications to the registration ROI were made (mainly reduction of the vertical extent) after which the registration was visually determined to be successful in all cases.

In case of repeated measurements, the anatomical scans of the two scan sessions were registered with each other using an initial rigid transformation model followed by the intrascan B-spline registration method described above.

T_1 and T_2 mapping

T_1 and T_2 fits were performed with the methods described in the section "T_1 and T_2 fitting."

This was done only in a user-defined ROI, which was selected as follows. For the volunteer data, a series of five nonadjacent slices were selected from the common carotid artery. In the axially reformatted data, ROIs were drawn in the carotid vessel wall and muscle as indicated in Figure 4a.

The same ROIs were then used to calculate slice-averaged T_1 and T_2 values of both baseline and the registered repeat scans. More specifically, we used the CRLB-weighted mean $\overline{\psi_{\mathrm{CRLB}}}$ (where ψ is T_1 or T_2) to take into account the reliability of each individual voxel-wise fit:

$$\overline{\psi_{\mathrm{CRLB}}} = \frac{\sum_{x\in\Omega}\psi(x)/\mathrm{CRLB}(\psi(x))}{\sum_{x\in\Omega}1/\mathrm{CRLB}(\psi(x))}, \qquad [3]$$

where Ω is the ROI in which the weighted mean is computed and $\mathrm{CRLB}(\psi(x))$ extracts the component corresponding to ψ from the diagonal of the CRLB matrix (23) of the parameter vector $[\boldsymbol{A}(\boldsymbol{x}), \boldsymbol{T}_1(\boldsymbol{x}), \boldsymbol{T}_2(\boldsymbol{x})]^{\boldsymbol{T}}$.

In the patient data, main areas of atherosclerotic plaque were clearly visible due to inward and/or outward remodeling of the vessel wall. Two ROIs within different plaque areas were drawn on axial reconstructions of the data. From the corresponding T_1 and T_2 maps, mean T_1 and T_2 values were calculated within these ROIs.

Statistical Analysis

Statistical analysis was performed only on the volunteer data. To investigate the effect of intrascan registration, for each ROI the median was taken of all $\sqrt{CRLB}$ of the voxelwise T_1 and T_2 estimates. The $\sqrt{CRLB}$ predicts the standard deviation of the maximum likelihood estimates, thus an improvement of that value indicates improved precision. Incorrect registration typically will cause larger CRLB values due to reduced fit quality (30). A paired Student's t-test was used to compare the $\sqrt{CRLB}$ with and without registration. Furthermore, the repeatability of slice-averaged T_1 and T_2 estimation was tested using an analysis of variance (ANOVA) with repeated measures with slice position as between-subject factor. In addition, Bland-Altman plots were constructed by calculating the relative difference in T_1 and T_2 between all paired measurements as function of their mean values (31). This allowed assessment of the measurement repeatability for T_1 and T_2 estimation, for which we calculated the between-session coefficient of variation (CV) (32).

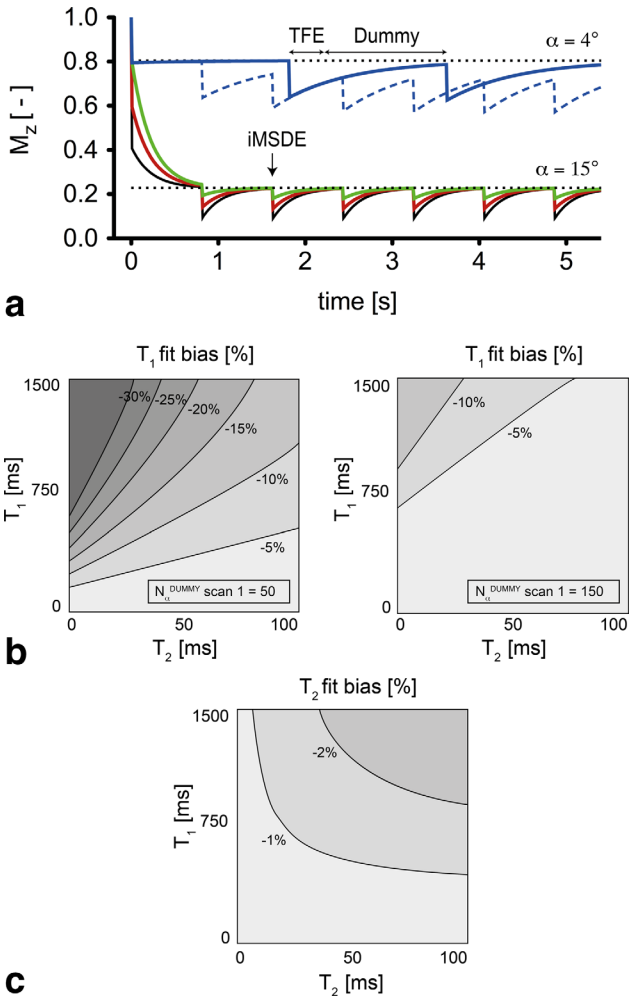

FIG. 2. Simulations. Result of Bloch simulations to assess the accuracy of T_1 and T_2 estimation. **a:** Example of longitudinal magnetization (M_z) time-course during the sequence for $T_1 = 1000$ ms and $T_2 = 50$ ms. Scans 1–4 are illustrated in blue, green, red and black, respectively. The arrow indicates the timing of the iMSDE prepulse. For scan 1 (blue), both $N_\alpha^{DUMMY} = 50$ (dashed) and $N_\alpha^{DUMMY} = 150$ (solid) are shown. The theoretical steady-state magnetization for both flip angles is indicated by the dotted lines. **b,c:** Relative bias in T_1 and T_2 estimation as function of their simulated input values. Note the lower underestimation of T_1 if $N_\alpha^{DUMMY} = 150$ is used for scan 1.

RESULTS

Simulations and Phantom Experiments

The time course of the longitudinal magnetization (M_z) during the sequence is shown in Figure 2a. A pseudo steady-state condition is formed, in which M_z is decreased during each iMSDE prepulse due to T_2 relaxation. Only in the case that sufficient dummy pulses are applied after TFE read-out, steady-state conditions satisfying the Ernst-equation (dotted line) are restored.

While for scan 1, this is only possible for a high number of dummy pulses, less dummy pulses are needed for

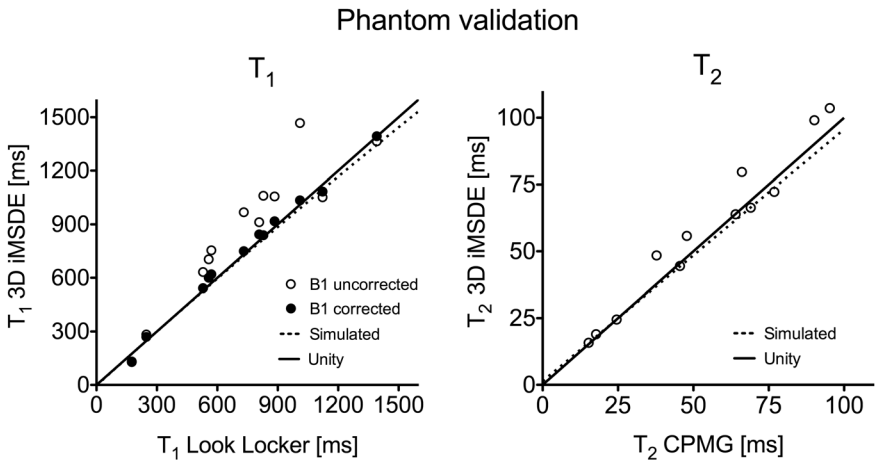

FIG. 3. Phantom measurements. Comparison of phantom T_1 and T_2 estimates using the 3D carotid sequence and gold standard methods. Simulations results based on the reference values are indicated with the dotted line. The solid line represents $y = x$.

the high flip angle scans (no. 2–4). Total scan time, therefore, varies between the different scans (see also Table 1). Figure 2b shows the relative bias in T_1 and T_2 estimation as function of its simulation input value for a small and large number of dummy pulses (50 versus 150).

As expected, the use of more dummy pulses will decrease the bias of T_1 estimation, because more time is available to reach steady-state conditions. For $N_\alpha^{DUMMY} = 150$, T_1 underestimation remains below 10% within the expected physiological range of T_1 and T_2 values. Finally, it was shown that the bias in T_2 estimation is small, almost independent of reference T_1 and T_2 (Fig. 2c).

Figure 3 shows the results of the phantom experiments. T_1 and T_2 values of the phantoms resulting from IR-Look Locker and CPMG sequences were in the range of 150–2000 ms and 15–100 ms, respectively. The estimated T_1 values clearly demonstrate the need for B_1 correction. In this case, T_1 values from the 3D carotid sequence were in very good agreement with reference values ($R^2 = 0.99$). T_2 estimation was independent of B_1 correction and also agreed very well with gold standard measurements ($R^2 = 0.96$).

In Vivo Measurements

Volunteer data

An example of in vivo images using the proposed 3D carotid T_1 and T_2 mapping protocol is shown in Figure 4a. Because of the isotropic voxel size of 0.7 mm, high-resolution images could be reconstructed in any direction. The coronal view shows the whole length of the carotid artery, while axial views represent cross-sections at specific locations. Blood suppression using the iMSDE prepulse proved effective, even in regions around the bifurcation. Different contrast obtained by the four protocol scans (Table 1) can be roughly identified as proton density weighted (scan 1), T_1-weighted (scan 2) and T_2-weighted (scan 3–4). Figure 4b shows quantitative T_1

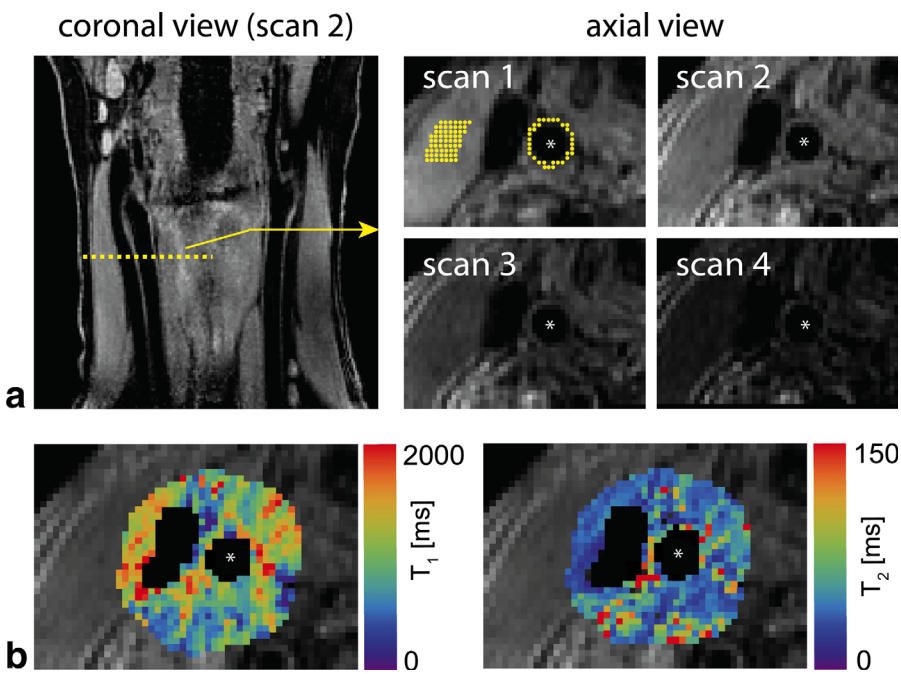

FIG. 4. Carotid artery T_1 and T_2 mapping in healthy volunteers. **a:** T_1- and T_2-weighted images corresponding to scan 1–4 (Table 1). Examples of muscle and carotid ROIs used for quantitative analysis are indicated in yellow. In axial views, the carotid artery lumen is marked by *. **b:** Carotid artery T_1 and T_2 maps of a healthy volunteer, calculated from the images in panel A. Note that T_1 and T_2 values are only estimated within the registration mask.

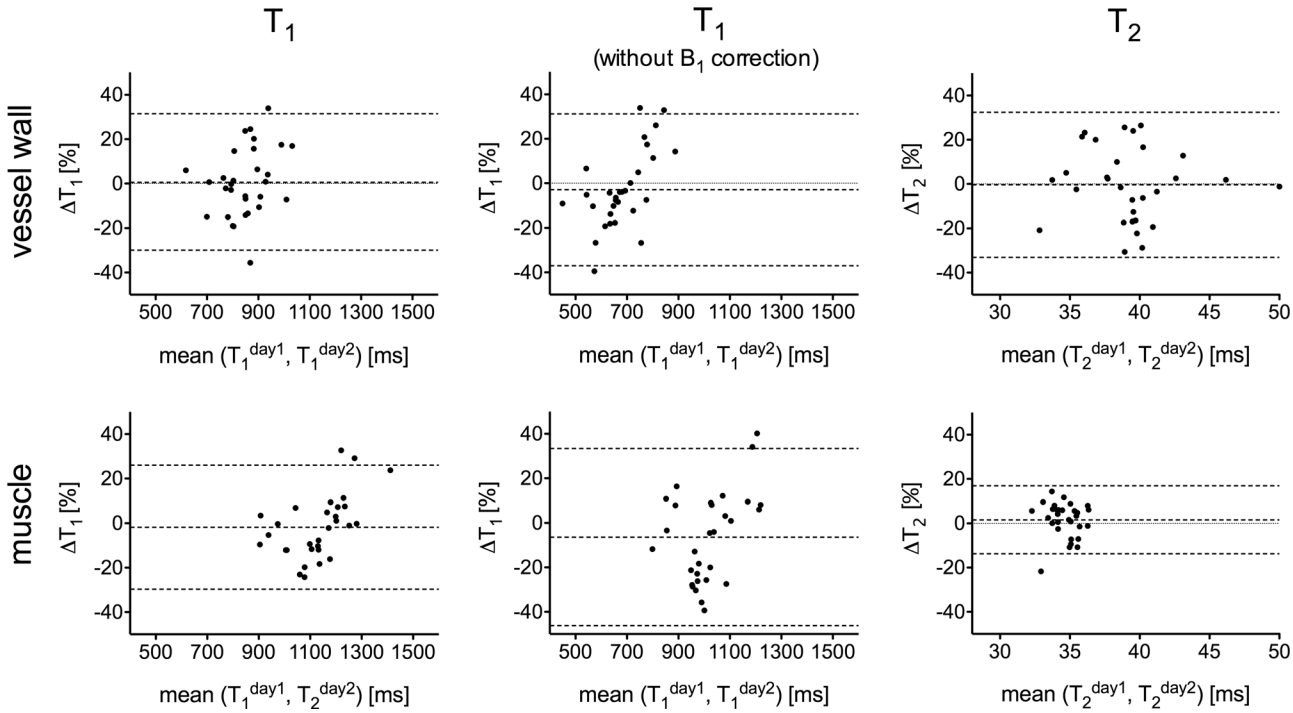

FIG. 5. Repeatability of T_1 and T_2 measurements. Bland-Altman plots showing the repeatability of T_1 and T_2 when measured at two different sessions. The relative difference of the two measurements is plotted against their respective means. Dashed lines indicate the means and 95% confidence intervals for $\Delta T_{1,2}$ between different sessions.

and T_2 maps from the images in Figure 4a. The anatomical structures including the carotid vessel wall can be nicely appreciated, which means that voxel-wise fitting of carotid T_1 and T_2 values is feasible after registration of the intrasession scans. Note that a few outliers are present in the T_1 and T_2 maps at locations where the fit was not reliable (red points in the overlay). These voxels are typically characterized by a high CRLB, and are thus weighted less in the computation of the mean T_1 and T_2 over an ROI. For carotid vessel wall, mean T_1 and T_2 values at baseline were 844 ± 96 ms and 39 ± 5, respectively, while corresponding values for muscle tissue were 1137 ± 110 ms and 34 ± 2.

For the vessel wall, registration of scans 1–4 before fitting resulted in a significant decrease in the median $\sqrt{CRLB}$ of voxelwise estimates of T_1 (143 ± 41 vs. 228 ± 105 ms; $P < 0.01$) and T_2 (9 ± 4 vs. 11 ± 5 ms; $P < 0.05$). In muscle, $\sqrt{CRLB}$ values for voxelwise T_1 and T_2 estimates were 72 ± 21 ms and 2.5 ± 1 ms, respectively, which were only marginally different from values without the use of registration. ANOVA with repeated measurements showed no significant differences between baseline and follow-up measurements, as well as no effect of slice position on mean T_1 and T_2 values. In Figure 5, Bland-Altman plots further illustrate the repeatability of the proposed method. CV values of T_1 were 11% and 12.0% for vessel wall and muscle tissue, respectively, while corresponding CR values for T_2 were 12% and 6%. Without B_1 correction, CV values for T_1 estimation were higher (vessel wall: 12%; muscle tissue: 15%). More importantly, absolute T_1 values without B_1 correction (vessel wall: 686 ± 79; muscle: 1044 ± 114) were significantly different ($P < 0.01$) from previously mentioned values. In correspondence with phantom experiments, B_1 correction had no effect on T_2 estimation.

Patient data

Figure 6 shows results for a patient with a known history of atherosclerosis. From the anatomical data (Fig. 6a), distinct areas of plaque burden could be observed around the right carotid bifurcation, which for clarification are delineated in axial reconstructions (reco 2 & 3).

Most notably, strong hyperintensities were seen in the internal carotid artery (reco 2). These regions showed strongly reduced values on coronal and axial T_1 maps (198 ± 26 ms), but also increased T_2 values (51 ± 4 ms) as compared to volunteer data. In another region of severe outward remodeling within the bifurcation (reco 3), T_1 and T_2 values were 716 ± 63 ms and 57 ± 7 ms, respectively, of which only T_2 was high compared with values in volunteers.

DISCUSSION

In this study, we presented a novel method for T_1 and T_2 quantification in the carotid artery using a single basic sequence design. This method combines variable flip angle 3D gradient-echo imaging with variable TE^{prep} iMSDE blood suppression. Through phantom studies and simulations, we showed that by applying the appropriate number of dummy pulses after signal acquisition, the acquired signal represents a T_2-weighted version of the T_1-weighted steady-state condition satisfying the Ernst equation, thereby allowing simultaneous estimation of T_1 and T_2. The use of dummy pulses to ensure

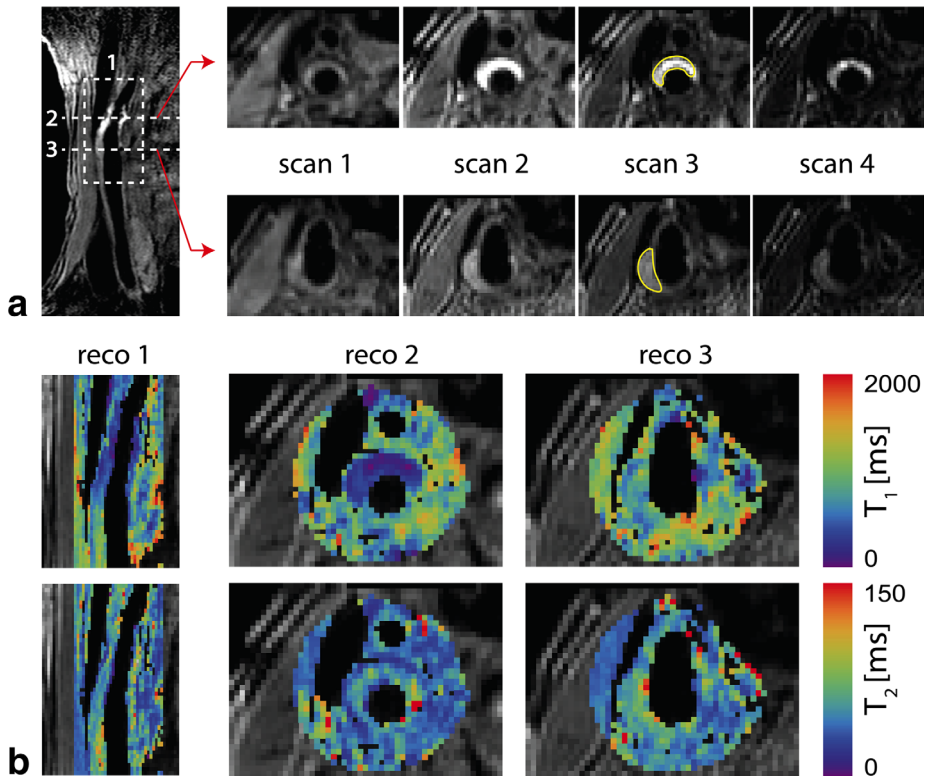

FIG. 6. Carotid artery T_1 and T_2 mapping in an atherosclerotic patient. **a:** Coronal (scan 2 only) and axially reconstructed (scans 1–4) T_1- and T_2-weighted images. Plaque regions were present around the right carotid bifurcation and indicated in yellow in the axial views. **b:** Coronal (reco 1) and axial (reco 2 and 3) T_1 and T_2 maps corresponding to the reconstruction views indicated in panel A. Regions of abnormal T_1 and/or T_2 could be associated with regions of severe plaque burden.

steady-state conditions inevitably leads to a substantial increase in imaging time. However, we showed that a high number of dummy pulses was only needed for the low flip angle scan. This kept the total imaging time for all scans (including reference scan and B_1 mapping) below 25 min. This is not much longer than a 2D multicontrast protocol consisting of a T_1-weighted, T_2-weighted and proton density-weighted scan, especially considering the fact that the latter has very limited coverage along the length of the carotid artery. A possible strategy that could allow considerable acceleration of the current method is the use of compressed sensing, for which promising results have already been obtained in carotid artery imaging applications (33,34). This might also allow acquisition of more scans to improve accuracy of T_1 and T_2 estimation. Finally, the transient effect of dummy pulses (or even a waiting time) might be incorporated into the signal model (Eq. [1]), which could enable us to choose the number of dummy pulses and their flip angles to maximize SNR efficiency.

In vivo T_1 and T_2 mapping of the carotid artery has been considered a major challenge, especially in combination with black-blood imaging, which is crucial for optimal vessel wall/lumen contrast and avoiding flow artifacts. Several other methods for blood suppression are proposed in literature that differ from the one used in this study. In multicontrast imaging, double/quadruple inversion recovery (DIR/QIR) prepulses are commonly used, for which blood suppression depends on specific timing of the acquisition with respect to T_1 relaxation. Although this approach is very efficient in 2D imaging, it has been shown to have very poor performance when combined with 3D imaging, especially in regions of slow flow (35). The same is true when performing blood suppression through saturation of inflowing blood by slice selective 90° pulses, because these need to be applied outside of the 3D imaging volume. In pilot experiments, we additionally found that this approach leads to large underestimation of T_1, most probably due to magnetization transfer effects (36). More recently, a novel blood suppression method using DANTE preparation was proposed (16,37). Although this also seems a promising candidate for quantitative imaging applications, the signal after preparation depends on the ratio of T_1 over T_2, which complicates accurate estimation of both parameters. In this study, the use of motion-sensitizing gradients resulted in excellent blood suppression in volunteers and patients as can be seen from Figures 4 and 6. However, our choice of a relatively low first-order gradient moment (to achieve a short TE^{prep}) might compromise blood suppression in cases of severe stenotic regions where recirculation and stasis can occur. Due to partial volume effects, this could affect T_1 and T_2 quantification close to the lumen. This effect, however, may be small due to strong saturation of stagnant blood (with high T_1) by the continuous 3D volume excitation.

Image registration of all T_1-weighted and T_2-weighted scans (scan no. 1–4) proved crucial for vessel wall T_1 and T_2 quantification. This was shown by a significant decrease in the $\sqrt{CRLB}$ values for voxelwise T_1 and T_2 estimation. Whereas we chose to register all scans to a separate anatomical reference, recently alternative group wise registration methods were proposed avoiding the need for choosing a target image (38). Repeatability of vessel wall T_1 and T_2 values was determined by

scanning healthy volunteers on two different days, both resulting in CV values of around 10–12%. As expected, these values are somewhat higher as compared to variable flip angle T_1 and T_2 mapping in the brain (CV = 6–8%; Deoni et al.) (9); however, in other anatomies such as cartilage tissue, similar values were found (CV = 11%; Siversson et al.) (39). Furthermore, CV values reported for other quantitative imaging parameters in carotid artery imaging were similar or higher, such as lipid core/calcification volume characterization with multicontrast MRI (CV = 10–30%; Li et al, Saam et al) (8,40).

In the current method, no cardiac triggering was used, because it was not possible to make the number of dummy pulses dependent on the cardiac cycle length, e.g. two RR intervals for scan 1 and one RR for scans 2–4. However, this could be considered as a limitation of the current method, because omitting cardiac triggering will decrease the effective resolution of the sequence as result of vessel wall movement due to blood pulsation. This therefore may be a source of variability in our T_1 and T_2 values. Another limitation of the study is that we did not perform interobserver analysis with respect to T_1 and T_2 quantification. However, unlike qualitative methods based on visual assessment of relative signal differences, our method provides quantitative data on vessel wall structure computed in a largely automated manner. Minimal user-input was needed for registration, where only ROIs around the carotid and muscle tissue were drawn. This therefore adds almost no variation to the final quantitative values.

Specifically for T_1 estimation, better results were obtained by including correction for the spatially varying B_1 field. The actual flip angle mapping method used in this study has no black-blood properties and poor vessel wall delineation. B_1 variations, however, are rather smooth across the imaging volume and when properly masking the acquired B_1 map, it can effectively be used for T_1 estimation. We found that mean values for the B_1 correction factor (κ^{scale}) were 0.90 ± 0.05 and 0.95 ± 0.06 for vessel wall and muscle, resulting in underestimation of T_1 when B_1 correction is not performed. We performed additional experiments (data not shown) in four healthy volunteers, where we determined T_1 and T_2 of sternocleidomastoid muscle using the same reference methods as those in phantom experiments (2D Look Locker and 2D CPMG), which are robust against B_1 variations. These experiments resulted in T_1 and T_2 values of 1134 ± 21 ms and 34 ± 0.6 ms, which are in striking accordance with those determined by our 3D carotid sequence after B_1 correction.

Quantitative data of a patient revealed clear alterations of T_1 and T_2 in regions of atherosclerotic plaque. In a specific region (Figure 6, reco 2), a highly decreased T_1 (198 ms), accompanied by a slightly increased T_2 (51 ms) most probably reflected the presence of intraplaque hemorrhage (IPH). In contrast, another region (Figure 6, reco 3) displaying increased T_2 (57 ms) without clear alterations in T_1 (716 ms) can most likely be associated with loose matrix tissue (41). However, because no histological data was available, it was beyond the scope of this study to make definite conclusions about the exact phenotype of this particular plaque.

Currently we are performing repeated measurements in a larger group of atherosclerotic patients to reveal whether the use of quantitative imaging techniques helps improving repeatability of plaque characterization (pilot data shown in Supporting Figure S1, which is available online). Additional correlation with consensus readings based on multicontrast imaging or histological evaluation will also be particularly relevant for the use of quantitative data in automatic plaque segmentation software (42,43).

CONCLUSIONS

A novel protocol for quantitative 3D carotid T_1 and T_2 mapping using iMSDE black-blood 3D gradient echo imaging with variable flip angle and variable TE^{prep} acquisitions proved feasible. Registration of intrasession scans improved the precision in T_1 and T_2 estimation. Future work will focus on acquisition acceleration, as well as applying the protocol in a large number of patients to correlate T_1 and T_2 values to the presence of specific plaque components. We believe this method can be a powerful tool for monitoring plaque progression in atherosclerotic patients.

ACKNOWLEDGMENTS

The authors acknowledge Dennis Heijtel for assisting in sequence implementation. Also, we thank Henk Smit and Diederik van Wijk for their insightful discussions.

APPENDIX : A

The nonlinear optimization problem given in Eq. [2] was initialized with the following procedure. Initial values for T_1 were obtained from the scans with identical TE^{prep} (scans 1 and 2) by linearizing Eq. [1]:

$$M^{SS}(\sin\alpha)^{-1} = M^{SS}(\tan\alpha)^{-1}E_1 + B \quad [3]$$

$$B = A(1 - E_1)e^{-TE^{prep}/T_2} \quad [3b]$$

$$E_1 = e^{-TR/T_1}. \quad [3c]$$

After substituting the observed image intensities, B and E_1 were solved from the linear system (Eq. [3]). Next, T_1 was solved from E_1 with Eq. [3b]. These initial T_1 values were clamped between 250 and 3000 ms to avoid erroneous initialization due to noise. Initial values for T_2 were obtained by linearizing Eq. [1] for the scans with identical α (scans 2–4):

$$\ln M^{SS} = C - \frac{1}{T_2}TE^{prep} \quad [4]$$

$$C = \ln\left(A\frac{1 - E_1}{1 - E_1\cos\alpha}\right)\sin\alpha \quad [4b]$$

where $1/T_2$ and C were estimated with a linear least squares estimator. This initial T_2 was clamped between 20 and 100 ms. The initial value of A is given by $\max\left[\min\left[e^C, 10^5\right], B\right]$. A constant initial σ is given by the mean over the scans of the median absolute initial residuals within the foreground mask of each scan. Starting from these initial values, the optimization in Eq. [2] is performed with a Newton method where the steps are

approximated by a preconditioned conjugate gradient method (44). The fitting procedure was implemented in MATLAB with custom routines.

APPENDIX : B

B_1 mapping as used in this study was based on an alternating TR (TR_1 and TR_2) steady-state gradient echo sequence producing two separate images (S_1 and S_2), whose ratio can be used as estimator for α independent of T_1 (26).

First, the two images resulting from the B_1 mapping acquisition were resampled with cubic b-spline interpolation to the same grid as the 3D iMSDE reference scan. Next, a foreground mask was constructed from the reference scan and the two resampled images, by selecting all voxels that in all scans have an intensity above 20% of the 95-percentile intensity. The final mask M is created by pruning the initial mask by a few voxels to keep only regions in which the values are not distorted due to flow or edge artifacts. Within this mask, first the correction factor κ^{init} was computed for each voxel $\mathbf{x}$ independently as follows:

$$\kappa^{init}(\boldsymbol{x}) = \begin{cases} \arccos\left(\dfrac{rn-1}{n-r}\right)\alpha_{nom}^{-1} & \boldsymbol{x} \in M \\ 0, & \boldsymbol{x} \notin M \end{cases} \quad [5]$$

where $r = S_2/S_1$, $n = TR_2/TR_1$ and α_{nom} is the nominal flip angle prescribed for the B_1 mapping scan. The final correction factor map, κ^{scale} is obtained by

$$\kappa^{scale} = \frac{\kappa^{init} * F}{M * F}, \quad [6]$$

which is the normalized convolution of κ^{init} with $F(\boldsymbol{x}) = f(x_1)f(x_2)f(x_3)$, with $f(x) = (1+x^2)^{-1}$. It was observed that the resulting κ^{scale} reasonably interpolated the acquired B_1 correction maps. For T_1 and T_2 mapping with B_1 correction, for each voxel the flip angles used in Eq. [2] were scaled by κ^{scale}.

REFERENCES

1. Takaya N, Yuan C, Chu BC, et al. Association between carotid plaque characteristics and subsequent ischemic cerebrovascular events - a prospective assessment with MRI - initial results. Stroke 2006;37: 818–823.
2. Esposito-Bauer L, Saam T, Ghodrati I, Pelisek J, Heider P, Bauer M, Wolf P, Bockelbrink A, Feurer R, Sepp D, et al. MRI plaque imaging detects carotid plaques with a high risk for future cerebrovascular events in asymptomatic patients. Plos One 2013;8:e67927.
3. Gupta A, Baradaran H, Schweitzer AD, Kamel H, Pandya A, Delgado D, Dunning A, Mushlin AI, Sanelli P. Carotid plaque MRI and stroke risk - a systematic review and meta-analysis. Stroke 2013;44: 3071–3077.
4. Moody A. Stroke: cause and effect - seek and ye shall find. JACC Cardiovasc Imaging 2012;5:406–408.
5. Cai JM, Hastukami TS, Ferguson MS, Small R, Polissar NL, Yuan C. Classification of human carotid atherosclerotic lesions with in vivo multicontrast magnetic resonance imaging. Circulation 2002;106: 1368–1373.
6. Fayad ZA, Fuster V. Clinical imaging of the high-risk or vulnerable atherosclerotic plaque. Circ Res 2001;89:305–316.
7. Chu B, Phan BAP, Balu N, Yuan C, Brown BG, Zhao X-Q. Reproducibility of carotid atherosclerotic lesion type characterization using high resolution multicontrast weighted cardiovascular magnetic resonance. J Cardiovasc Magn Reson 2006;8:793–799.
8. Li FY, Yarnykh VL, Hatsukami TS, Chu BC, Balu N, Wang JN, Underhill HR, Zhao XH, Smith R, Yuan C. Scan-rescan reproducibility of carotid atherosclerotic plaque morphology and tissue composition measurements using multi-contrast MRI at 3T. J Magn Reson Imaging 2010;31:168–176.
9. Deoni SCL, Williams SCR, Jezzard P, Suckling J, Murphy DGM, Jones DK. Standardized structural magnetic resonance imaging in multicentre studies using quantitative T1 and T2 imaging At 1.5 T. Neuroimage 2008;40:662–671.
10. Rogers T, Dabir D, Mahmoud I, Voigt T, Schaeffter T, Nagel E, Puntmann VO. Standardization of T1 measurements with MOLLI in differentiation between health and disease - the consept study. J Cardiovasc Magn Reson 2013;15:78.
11. Toussaint JF, Lamuraglia GM, Southern JF, Fuster V, Kantor HL. Magnetic resonance images lipid, fibrous, calcified, hemorrhagic, and thrombotic components of human atherosclerosis in vivo. Circulation 1996;94:932–938.
12. Biasiolli L, Lindsay AC, Chai JT, Choudhury RP, Robson MD. In-vivo quantitative T2 mapping of carotid arteries in atherosclerotic patients: segmentation and T2 measurement of plaque components. J Cardiovasc Magn R 2013:15.
13. Newbould RD, Owen DRJ, Shalhoub J, Brown AP, Gambarota G. Motion-sensitized driven equilibrium for blood-suppressed T2* mapping. J Magn Reson Imaging 2011;34:702–709.
14. Sharkey-Toppen TP, Mihai G, Maiseyeu A, Tran T, Clymer BD, Simonetti OP, Raman SV. Improved in vivo human carotid artery wall T2* estimation. Magn Reson Imaging 2013;31:44–52.
15. Coolen BF, Heijtel DF, Potters WV, Nederveen AJ. 3D carotid wall T1 quantification using variable flip angle 3D merge with steady-state recovery. In Proceedings of the 21s t Annual Meeting of ISMRM, Salt Lake City, Utah, USA, 2013. Abstract 880.
16. Li L, Biasiolli L, Robson MD, Miller KL, Jezzard P. Fast relaxation time mapping in human carotid artery wall using black-blood DANTE 2D turbo spin echo. In Proceedings of the 21st Annual Meeting of ISMRM, Salt Lake City, Utah, USA, 2013. Abstract 4541.
17. Deichmann R, Haase A. Quantification of T_1 values by snapshot-FLASH NMR imaging. J Magn Reson 1992;96:608–612.
18. Deoni SCL, Rutt BK, Peters TM. Rapid combined T_1 and T_2 mapping using gradient recalled acquisition in the steady state. Magn Reson Med 2003;49:515–526.
19. Wang JN, Yarnykh VL, Yuan C. Enhanced image quality in black-blood MRI using the improved motion sensitized driven equilibrium (Imsde) sequence. J Magn Reson Imaging 2010;31:1256–1263.
20. Giri S, Chung YC, Merchant A, Mihai G, Rajagopalan S, Raman SV, Simonetti OP. T_2 Quantification for improved detection of myocardial edema. J Cardiovasc Magn Reson 2009;11:56.
21. Coolen BF, Simonis FFJ, Geelen T, Moonen RPM, Arslan F, Paulis LEM, Nicolay K, Strijkers GJ. Quantitative T2 mapping of the mouse heart by segmented MLEV phase-cycled T2 preparation. Magn Reson Med 2014;72:409–417.
22. Poot DHJ, Klein S. Detecting statistically significant differences in quantitative MRI experiments, applied to diffusion tensor imaging. IEEE Trans Med Imaging 2014. [Epub ahead of print].
23. Van Der Bos A. Parameter estimation for scientists and engineers. New York: Wiley; 2008.
24. Deoni SCL. High-resolution T_1 mapping of the brain at 3T with driven equilibrium single pulse observation of T_1 with high-speed incorporation of RF field inhomogeneities (DESPOT1-HIFI). J Magn Reson Imaging 2007;26:1106–1111.
25. Koning W, De Rotte AAJ, Bluemink JJ, Van Der Velden TA, Luijten PR, Klomp DWJ, Zwanenburg JJM. MRI of the carotid artery at 7 Tesla: quantitative comparison wth 3 Tesla. J Magn Reson Imaging 2015;41:773–780.
26. Yarnykh VL. Actual flip-angle imaging in the pulsed steady state: a method for rapid three-dimensional mapping of the transmitted radiofrequency field. Magn Reson Med 2007;57:192–200.
27. Ikemoto Y, Takao W, Yoshitomi K, Ohno S, Harimoto T, Kanazawa S, Shibuya K, Kuroda M, Kato H. Development of a human-tissue-like phantom for 3T MRI. Med Phys 2011;38:6336–6342.
28. Klein S, Staring M, Murphy K, Viergever MA, Pluim JPW. Elastix: a toolbox for intensity-based medical image registration. IEEE Trans Med Imaging 2010;29:196–205.

29. Van'T Klooster R, Staring M, Klein S, Kwee RM, Kooi ME, Reiber JHC, Lelieveldt BPF, Van Der Geest RJ. Automated registration of multispectral MR vessel wall images of the carotid artery. Med Phys 2013;40:121904.
30. Bron EE, Van Tiel J, Smit H, Poot DHJ, Niessen WJ, Krestin GP, Weinans H, Oei EHG, Kotek G, Klein S. Image registration improves human knee cartilage T1 mapping with delayed gadolinium-enhanced MRI of cartilage (dGEMRIC). Eur Radiol 2013;23:246–252.
31. Bland JM, Altman DG. Measuring agreement in method comparison studies. Stat Methods Med Res 1999;8:135–160.
32. Bland JM, Altman DG. Measurement error. Br Med J 1996;312: 1654–1654.
33. Makhijani MK, Balu N, Yamada K, Yuan C, Nayak KS. Accelerated 3D MERGE carotid imaging using compressed sensing with a hidden Markov tree model. J Magn Reson Imaging 2012;36:1194–1202.
34. Li B, Dong L, Chen B, Ji SX, Cai WC, Wang Y, Zhang J, Zhang ZQ, Wang XY, Fang J. Turbo fast three-dimensional carotid artery black-blood MRI by combining three-dimensional MERGE sequence with compressed sensing. Magn Reson Med 2013;70:1347–1352.
35. Wang J, Yarnykh VL, Hatsukami T, Chu B, Balu N, Yuan C. Improved suppression of plaque-mimicking artifacts in black-blood carotid atherosclerosis imaging using a multislice motion-sensitized driven-equilibrium (MSDE) turbo spin-echo (TSE) sequence. Magn Reson Med 2007;58:973–981.
36. Coolen BF, Geelen T, Paulis LEM, Nauerth A, Nicolay K, Strijkers GJ. Three-dimensional T_1 mapping of the mouse heart using variable flip angle steady-state mr imaging. NMR Biomed 2010;24:154–162.
37. Li LQ, Miller KL, Jezzard P. DANTE-prepared pulse trains: a novel approach to motion-sensitized and motion-suppressed quantitative magnetic resonance imaging. Magn Reson Med 2012;68:1423–1438.
38. Huizinga W, Poot DHJ, Guyader JM, et al. Non-rigid groupwise image registration for motion compensation in quantitative MRI. In: Ourselin S, Modat M, editors. WSOB. London, UK: Springer; 2014. p 184–193.
39. Siversson C, Tiderius C-J, Neuman P, Dahlberg L, Svensson J. Repeatability of T1 quantification in dgemric for three different acquisition techniques: two-dimensional inversion recovery, three-dimensional look locker, and three-dimensional variable flip angle. J Magn Reson Imaging 2010;31:1203–1209.
40. Saam T, Kerwin WS, Chu B, et al. Sample size calculation for clinical trials using magnetic resonance imaging for the quantitative assessment of carotid atherosclerosis. J Cardiovasc Magn Reson 2005;7:799–808.
41. Saam T, Ferguson MS, Yarnykh VL, Takaya N, Xu D, Polissar NL, Hatsukami TS, Yuan C. Quantitative evaluation of carotid plaque composition by in vivo MRI. Arterioscler Thromb Vasc Biol 2005;25: 234–239.
42. Nieuwstadt HA, Geraerdts TR, Truijman MTB, Kooi ME, Van Der Lugt A, Van Der Steen AFW, Wentzel JJ, Breeuwer M, Gijsen FJH. Numerical simulations of carotid MRI quantify the acuracy in measuring atherosclerotic plaque components in vivo. Magn Reson Med 2014;72:188–201.
43. Liu WB, Balu N, Sun J, Zhao XH, Chen HJ, Yuan C, Zhao HL, Xu JR, Wang GZ, Kerwin WS. Segmentation of carotid plaque using multi-contrast 3D gradient echo MRI. J Magn Reson Imaging 2012;35: 812–819.
44. Nocedal J, Wright SJ. Numerical optimization. New York: Springer; 2000.

SUPPORTING INFORMATION

Additional Supporting Information may be found in the online version of this article.

Figure S1. Repeated carotid T_1/T_2 measurement in an atherosclerotic patient. Example of a repeated measurement (sessions 2 hours apart) in a patient with 30–70% stenosis, showing 3D iMSDE reference scan (left), T_1 map (middle) and T_2 map (right). Mean T_1 values in the plaque (white region) were 174 ms and 217 ms on Scan and Rescan, respectively. Corresponding T_2 values were 41 ms and 40 ms.